*Article*

# Fingering Instability of Binary Droplets on Oil Pool

**Koji Hasegawa *** and **Yuya Kishimoto**

Department of Mechanical Engineering, Kogakuin University, Tokyo 163-8677, Japan
* Correspondence: kojihasegawa@cc.kogakuin.ac.jp

**Abstract:** The interfacial instability of a complex fluid in a multiphase flow system is ubiquitous in both nature and industry. We experimentally investigated the spreading and interfacial instability dynamics of a binary droplet (a water and 2-propanol (IPA) mixture) on an immiscible (sunflower oil) pool. For droplets of 40 wt% IPA solution on sunflower oil, fingering instability occurred at the spreading liquid front. To reveal the interfacial characteristics of the spreading and fingering processes, we analyzed the interplay among the speed, diameter, and number of fingers on the spreading front. Based on our observations, the finger length, wavelength between the fingers, head length, and neck length were quantified. Our experimental results clearly demonstrate that fingering instability can be driven by the capillary effect for a liquid–liquid system as well as the Plateau–Rayleigh instability. We hope that our results will inspire further experimental and numerical investigations to provide deeper insights into the interfacial dynamics of multicomponent droplets in a liquid pool.

**Keywords:** fingering instability; binary droplets; droplet spreading

## 1. Introduction

The wetting, spreading of droplets, and the accompanying fingering instability have attracted considerable attention as natural phenomena and those that occur in various industries [1–9]. Understanding the interfacial dynamics is crucial for exploring the impingement of droplets on solid and liquid substrates [10–13]. To better understand spreading characteristics, the evaporation-induced Marangoni effect has been extensively investigated over the past few decades [14–35]. For solid substrates, Mouat et al. [20] investigated contact line dynamics and fingering patterns in volatile liquid mixtures on a silicon wafer. They demonstrated two distinct regimes of interfacial instability: surface wetting and solutal Marangoni forces. The spontaneous spreading of a thin volatile film along the surface of a liquid layer with a higher surface tension has been studied experimentally and theoretically by Troian et al. [21–24]. In the case of a deep liquid layer, although previous studies of the spreading dynamics of non-volatile immiscible thin films on a deep liquid layer have shown that the spreading front advances in time as $t^{3/4}$ as predicted by laminar boundary layer theory, they found that the leading edge of volatile immiscible spreading films also advances with time as a power law, $t^{\alpha}$, where $\alpha \sim 1/2$ [22]. This indicates that the differences in liquid vapor pressure or spreading coefficient can affect the velocity of the spreading front and suggests the presence of a universal scaling law. A recent work by Keiser et al. [25] revealed the instability that was observed when a two-component drop of water and volatile alcohol is deposited on a bath of sunflower oil. The drop temporarily spreads and spontaneously breaks up into thousands of tiny droplets owing to the Marangoni effect, which is induced by the evaporation of the IPA component. To understand the spreading dynamics caused by the concentration gradient of the IPA–water interface, Kim et al. [26] analyzed the spreading owing to the solutal Marangoni effect in fully miscible liquids by employing a scaling analysis. Even for non-Newtonian fluids, Ma et al. [29] discussed fingering instability during Marangoni spreading on a deep layer of the polymer. For a surfactant-coated droplet, Matar and Troian [35] investigated the linear

stability of a coupled set of equations describing the Marangoni spreading of a surfactant monolayer on a thin liquid film. They found that the inclusion of additional forces acting on the surfactant-coated spreading film could form regions of unfavorable mobility gradients known to produce finger instabilities in other fluid flows.

Although several researchers have explored the dynamics of the spreading and fingering instabilities associated with the Marangoni effect, more quantitative and predictive insights into the interfacial instability during the spreading and self-atomization processes are needed. A better understanding of the spreading and fingering instability characteristics will enable the development of a promising atomization technology for a liquid–liquid interface that is easy to operate and can produce thousands of microdroplets within a short time. This study aimed to identify the spreading and fingering instability characteristics of an evaporating liquid pool. We visualized and quantified the dynamic behavior of IPA solution droplets on an oil pool. During the spreading process of the released droplet, the fingering instability in the circumferential and radial directions was characterized on the spreading front via the capillary and critical instability lengths. These experimental findings may also be relevant to other fascinating Marangoni-driven dynamics, such as the swimming of droplets [36] and particles [37], and other interfacial phenomena [38–42].

## 2. Materials and Methods

Figure 1 represents a schematic of the experimental setup in the present study. The experimental setup consisted of an oil pool in a Petri dish, a pipette for an injection of droplets, and a digital camera for a visualization. The droplets were placed manually on the oil pool. The droplet behavior was captured using a digital video camera (Nikon, D5600) backlit with an LED light (WTH-C2020, Nissin Electronics Co., Ltd., Hachioji, Japan). To enhance the contrast, the droplets were dyed blue using food coloring. The obtained images were processed using the ImageJ software (1.52v) to estimate the spreading and fingering instability of the droplets. In this study, a 40 wt% 2-propanol (IPA)/water mixture and sunflower oil were used as the droplet and pools, respectively. In a previous study [33], we investigated the speed dynamics of 20, 40, 60, and 80 wt% IPA solutions in sunflower oil. For the 20 wt% IPA solution, the released droplet floated on sunflower oil (no obvious change occurred even after 20 s of contact). For higher concentrations of IPA solution (i.e., 60 and 80 wt%), although spontaneous spreading and atomization were observed on the sunflower oil, the finger length was too short, and the atomized daughter droplet size was too small to observe and quantify the entire process. To better understand the spreading and fingering instability dynamics, we focused on the 40 wt% IPA solution. The depth of the oil pool was fixed at 10 mm. The inner diameter of each Petri dish was 85.7 mm. The droplets released on the oil pool are ≈2.0 mm in diameter. The ambient temperature and relative humidity were 25 °C and 50%, respectively. The droplet motion was recorded at 60 fps with a spatial resolution of ≈85 µm/pixel.
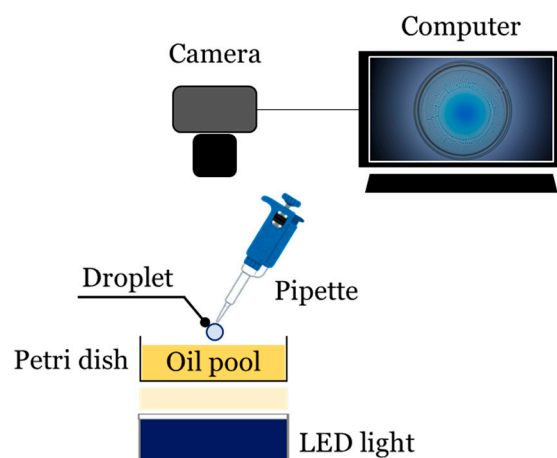


**Figure 1.** Schematic of the experimental setup.

Table 1 lists the thermophysical properties of the tested liquids. The density and kinematic viscosity of sunflower oil were measured. All surface tensions listed in Table 1 are the surface tensions between each liquid and air.

**Table 1.** Thermophysical properties of the test fluids.

| Test Sample | Density $\rho$ (kg/m$^3$) | Kinematic Viscosity $\nu$ (mm$^2$/s) | Surface Tension $\sigma$ (mN/m) |
|---|---|---|---|
| Water [1] | 997 | 0.89 | 72 |
| IPA [1] | 781 | 2.61 | 21 |
| Sunflower oil | 916 | 58 | 32 [2] |

[1] Ref. [43]. [2] Ref. [25].

## 3. Results and Discussion

### 3.1. Droplet Spreading

Figure 2 shows the effect of 40 wt% IPA solution on sunflower oil. After contact with oil (time $t$ = 0 s; Figure 2a), the released droplets started wetting and spreading within 1 s (Figure 2b). Fingering instability and atomization were observed after 6 s (Figure 2c). The spreading front reaches its maximum diameter after 12 s (Figure 2d). Subsequently, the spreading front gradually shrunk (Figure 2e) and finally vanished after 26 s (Figure 2f). During this process, the released droplet forms a wetting film that exhibits fingering at the spreading front. Furthermore, it is reasonable to assume that brightness corresponds to the IPA concentration distribution in the spreading film, allowing us to predict the concentration. The initial stage of droplet spreading ($\approx$6 s) is darker blue (higher IPA concentration) near the center of the spreading film, which gradually changes to a lighter shade of blue (lower IPA concentration) in the later stage ($\approx$26 s) with the evaporation of the IPA component. Based on these results, we quantified the brightness value to analyze the spreading behavior.
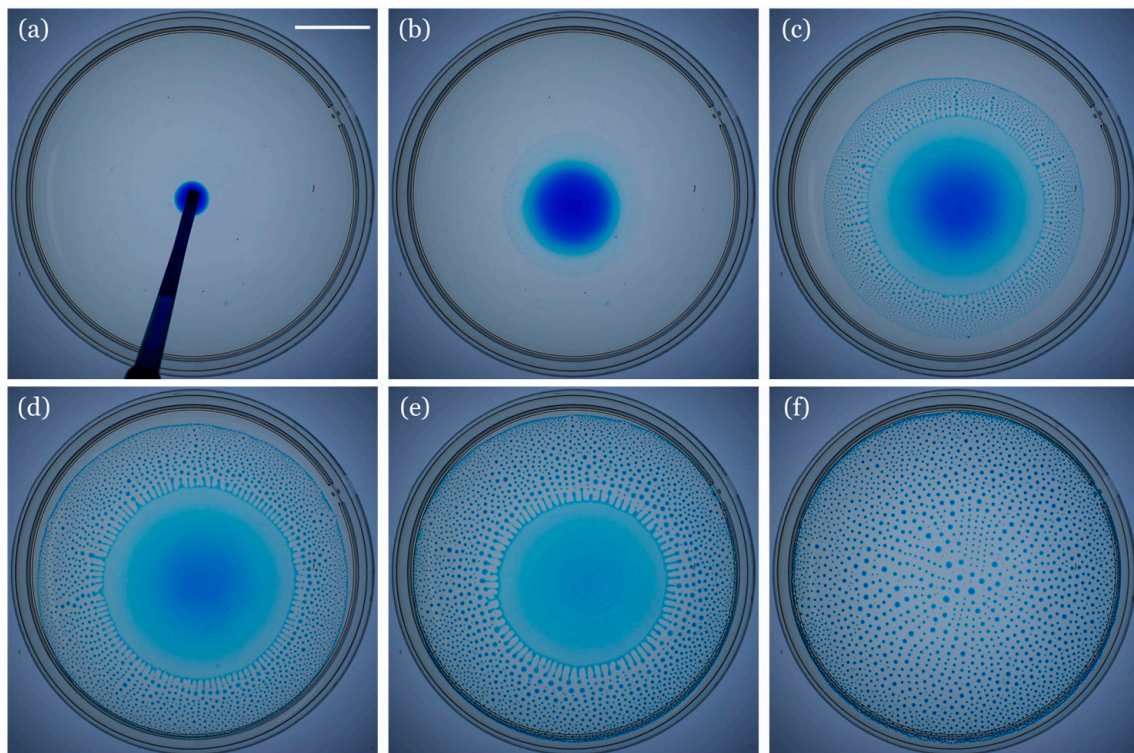


**Figure 2.** Snapshots of dyed 40 wt% IPA solutions on the sunflower oil for (**a**) $t$ = 0 s, (**b**) 1 s, (**c**) 6 s, (**d**) 12 s, (**e**) 18 s, and (**f**) 26 s, respectively. $t$ = 0 s indicates the time at which the droplet contacted the oil pool. Scale bar in (**a**): 20 mm.

Figure 3 represents the brightness information of the spreading films. The data for the spreading times of 1, 6, 12, and 18 s correspond to the snapshots in Figure 2. The brightness changed with time, as shown in Figure 3a, allowing us to quantify the position of the spreading front on the oil pool, which reached 12 mm at 1 s, 20 mm at 6 s, and 22 mm at 12 s, and shrank subsequently. The brightness fluctuation beyond the spreading front is due to the pinch-off of the droplets owing to the fingering instability. Figure 3b represents the brightness decay at the center of the spreading film ($R = 0$ mm in Figure 3a). The linear decrease in the brightness value was consistent with the IPA components in the spreading binary liquid film, which evaporated linearly with time. Consequently, the evaporation-induced Marangoni force can drive the spontaneous spreading and shrinking processes [29]. According to a previous analysis [25], it can be assumed that the spreading coefficient $S$ ($= \sigma_{oa} - \sigma_{sa} - \sigma_{so}$) [44] becomes positive for the 40 wt% IPA solution and increases with the increasing IPA concentration, forcing the droplets to stretch and spread to the outer edge in the early stage. The parameters $\sigma_{oa}$, $\sigma_{sa}$, and $\sigma_{so}$ represent the oil–air, solution–air, and solution–oil interfacial tensions, respectively. For lower concentrations of IPA solution (<35 wt%), the spreading coefficient was negative, and the droplet floated on the pool [29]. Notably, an appropriate amount of water ($\geq$35 wt% IPA solution) plays a critical role in the spontaneous spreading dynamics. In the present case, the surface tensions of sunflower oil and 40 wt% IPA solution in air are 32 and 25 mN/m, respectively, and the interfacial tension is approximately 3 mN/m [25]. Using these figures, the initial spreading coefficient in the present case can be $32 - (25 + 3) = 4$ mN/m. This indicates that the 40 wt% IPA solution spontaneously spreads over the sunflower oil pool initially.
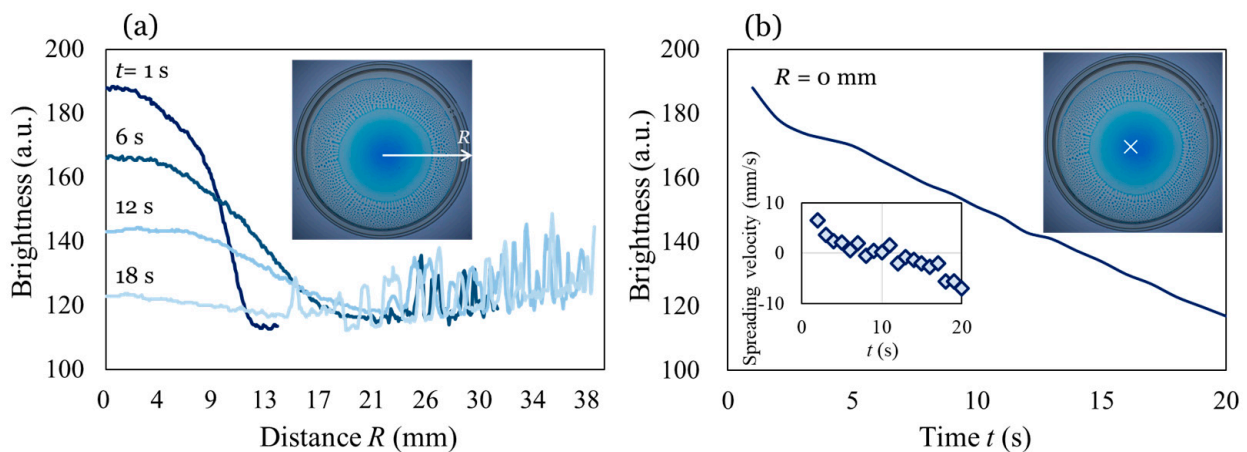


**Figure 3.** Brightness information obtained during the spreading of 40 wt% IPA solutions on sunflower oil. (**a**) Brightness profiles at 1, 6, 12, and 18 s. Inset: coordinates of the distance $R$. (**b**) Time evolution of the brightness at $R = 0$ mm (center of spreading film marked as $\times$). To eliminate the effects of the injection process, the brightness data from 1 s onwards are plotted. Inset: the film-spreading velocity.

Spontaneous spreading determines the contact line speed. The contact line speed affected the evaporation rate of the IPA component by increasing the surface area of the 40 wt% IPA solution in air on sunflower oil. Therefore, the evaporation of the IPA component can be enhanced using faster contact line speeds for a larger spreading coefficient (higher IPA concentration), resulting in a stronger Marangoni effect on the spreading film. To explain this quantitatively, we estimated the Marangoni velocity of the spreading film for a 40 wt% IPA solution. We assumed competition between Marangoni stress and viscous stress on the spreading film. The Marangoni and viscous stresses on the film can be described by $\frac{\Delta \sigma}{R_{max}}$ and $\mu_p \frac{V_m}{H}$, respectively. By balancing the tangential stresses at the interface, we derived the Marangoni velocity as shown in Equation (1).

$$V_m \sim \frac{\Delta \sigma H}{\mu_p R_{max}} \tag{1}$$

where $\Delta\sigma$ is the surface tension deference between the front and center of the spreading film due to the evaporation, $H$ is the oil-pool depth, $\mu_p$ is the viscosity of the sunflower oil, and $R_{max}$ is the maximum spreading radius. By substituting $\Delta\sigma \sim O(1)$ mN/m, $H = 10$ mm, $\mu_p = 63$ mPa·s, and $R_{max} = 45$ mm into Equation (1), we obtain a Marangoni velocity of $O(10^{-3})$ m/s. This estimate is in quantitative agreement with the film-spreading velocity shown in the inset of Figure 3b.

### 3.2. Fingering Instability on Spreading Front

During droplet spreading on the oil pool, fingering instability was generated on the spreading front, as shown in Figure 2c–e. Figure 4 represents the fingering dynamics as a function of the characteristic length. A typical snapshot of the fingering instability of one-quarter of a spreading film is shown in Figure 4a. The number of fingers increased and decreased with the droplet spreading and shrinking, respectively, as shown in Figure 4b. For one-quarter of the spreading area, when the spreading film was fully developed for $5\,\text{s} < t < 14\,\text{s}$, over 20 fingers were observed at the spreading front. Notably, capillary-driven fingering instability is strongly related to the evaporation of the IPA component. To reveal these fingering characteristics, we quantified the four characteristic lengths depicted in the inset of Figure 4a: finger length, $\lambda_r$; wavelength, $\lambda_\theta$; head length, $D$; and neck length, d. Figure 4c plots the time evolution of these characteristic lengths. For $\lambda_\theta$ and $d$, the experimental data was almost constant during the spreading process, while $\lambda_r$ and $D$ increased with time. This indicates that the instability mechanism must be distinguished between the circumferential and radial directions.
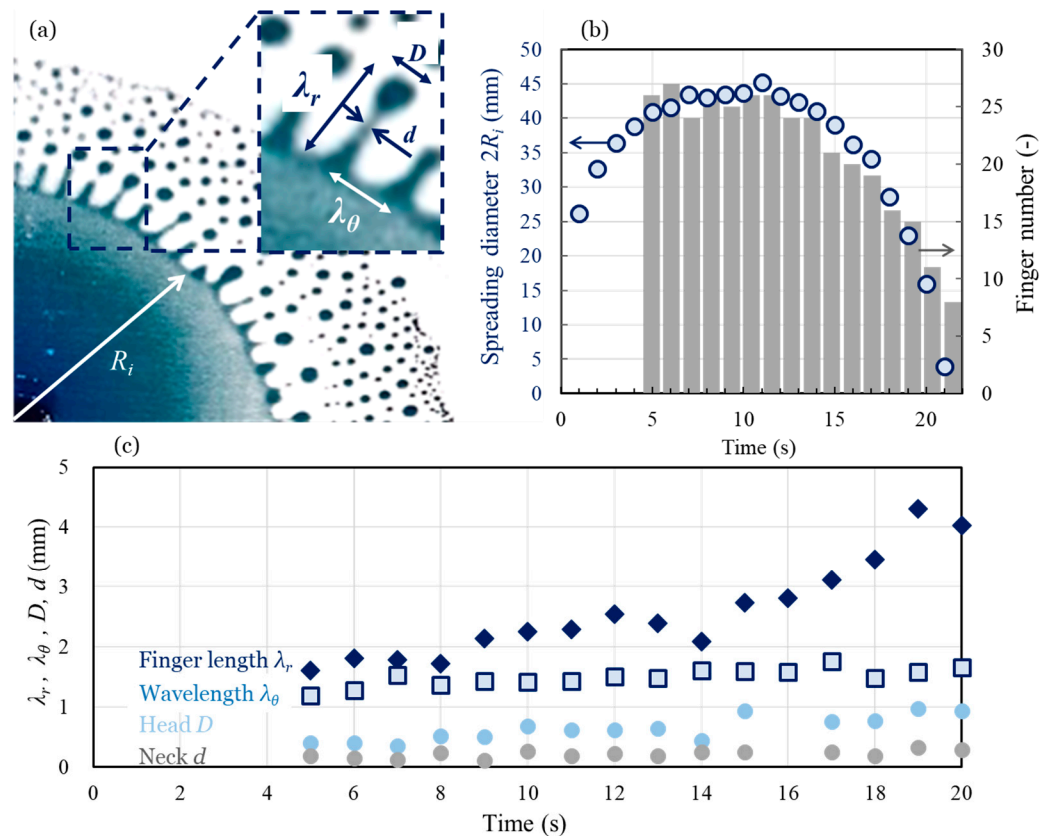


**Figure 4.** Fingering characteristics on the spreading front. (**a**) Snapshot of the fingering instability. $R_i$ represents the radius from the spreading center to the front. Four characteristic lengths are defined in the close-up view. (**b**) Relationship between the spreading diameter and finger number on the spreading front. (**c**) Time evolution of the finger length, wavelength, head length, and neck length.

For the circumferential direction, the capillary length of the liquid–liquid (IPA solution–sunflower oil) interface, $\lambda_c$ can be calculated using Equation (2) [1]:

$$\lambda_c \sim \sqrt{\frac{\sigma_{so}}{(\rho_o - \rho_{IPA})g}} \qquad (2)$$

where $\sigma_{so}$ is the interfacial tension between the IPA solution and sunflower oil, $\rho_o$ is the density of sunflower oil, $\rho_{IPA}$ is the density of IPA, and $g$ is the gravitational acceleration. Figure 5a shows the time evolution of the wavelength between the fingers in the circumferential direction. The wavelength was normalized to the capillary length, as described in Equation (2). For $\sigma_{so} \sim 3$ mN/m [25], $\rho_o = 916$ kg/m$^3$, $\rho_s = 781$ kg/m$^3$, and $g = 9.81$ m/s$^2$, the predicted wavelength of $\approx 1.5$ mm agrees well with the experimental data. This model allows us to conclude that a higher concentration of IPA leads to lower interfacial tension and wavelength [29]. In Figure 5, although we characterized the time evolution of the wavelength between the fingers in the circumferential direction by the capillary length for the liquid–liquid interface, the experimental data showed a slight increase with time. This may be due to the effect of evaporation on the interfacial tension caused by a change in the IPA concentration in the spreading film. To verify the effect of interfacial tension distribution by evaporation, future work is expected to measure the IPA concentration distribution during film spreading.
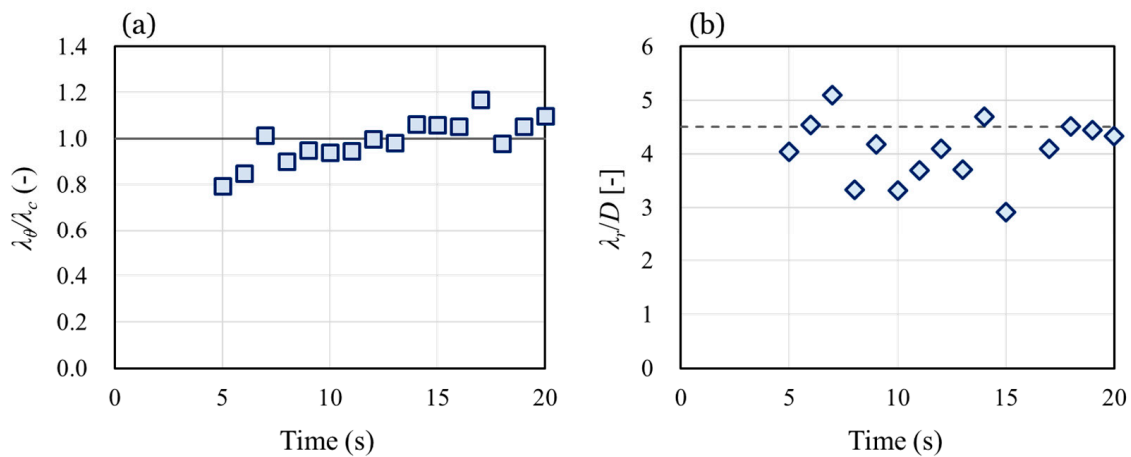


**Figure 5.** Time evolution of characteristic finger length in the (**a**) circumferential direction and (**b**) radial direction. The solid line in (**a**) and dashed line in (**b**) indicate the capillary length of the liquid–liquid (IPA solution–sunflower oil) interface predicted using Equation (2) and the most unstable wavelength predicted by the Plateau–Rayleigh instability in Equation (4), respectively.

In the radial direction, the pinch-off process is reminiscent of the classical Plateau–Rayleigh instability of liquid cylinders [45]. Based on this assumption, the experimental results were compared with those of the theoretical model. The key expression that describes the development of the Rayleigh–Plateau instability is the dispersion relation between the growth rate $\omega$ and wave number $k$ (=$2\pi/\lambda$, where $\lambda$ is the wavelength on liquid cylinder interface). For axisymmetric capillary waves on a liquid cylinder with radius $R_0$:

$$\omega^2 = \frac{\sigma}{\rho R_0^3} \frac{I_1(kR_0)}{I_0(kR_0)} kR_0 \left(1 - (kR_0)^2\right), \qquad (3)$$

where $\sigma$ is the surface tension of the liquid cylinder and $I_0$ and $I_1$ are the modified Bessel functions of the first kind. From this relationship, if the right-hand side of Equation (3) becomes positive ($kR_0 < 1$), the perturbation grows exponentially and eventually forces the system to become unstable. The fastest growing mode occurred for $kR_0 = 0.697$, i.e., when the wavelength of the disturbance $\lambda_{crit} \sim 9.02R_0$. By substituting $R_0 = D/2$ into $\lambda_{crit}/R_0 \sim 9.02$,

we calculated the critical wavelength of the Plateau–Rayleigh instability, $\lambda_{crit}$, according to Equation (4) [7,45].

$$\frac{\lambda_{crit}}{D} \sim 4.51, \tag{4}$$

Figure 5b shows the time evolution of the finger length in the circumferential direction. The finger length was normalized to the critical wavelength predicted using Equation (4). Our experimental results roughly agree with theoretical predictions. A reason for the slight difference between the experimental data and theoretical values is the interplay between the fingers. Although the Plateau–Rayleigh instability assumes only one liquid cylinder, multiple fingers exist, and neighboring fingers may dynamically interact in the present case. Another possible reason for this is the effect of the flow field on the spreading film. For an evaporation-driven flow near the spreading front, the flow fluctuation generated pressure fluctuations and enhanced the interfacial deformation for finger formation.

One fingering instability application resulted in tiny and myriad daughter droplets after the pinch-off. Figure 6a shows the generation frequency of daughter droplets owing to fingering instability. In this study, we analyzed five representative fingers. According to our results, the majority of the daughter droplets measured less than 1 mm, with frequencies in the range of 1–4 Hz. By counting the droplets produced from five representative fingers, Figure 6b shows the probability density function (PDF) histogram for the daughter droplet diameter. For all 131 data points associated with the five representative fingers, the average diameter and standard deviation of the daughter droplets were 0.7 and 0.2 mm, respectively. According to Figure 4b, nearly one-hundred fingers occupied the entire spreading front during the spreading phenomenon; therefore, the total number of daughter droplets can exceed 2000 for the entire spreading circle within tens of seconds [29].
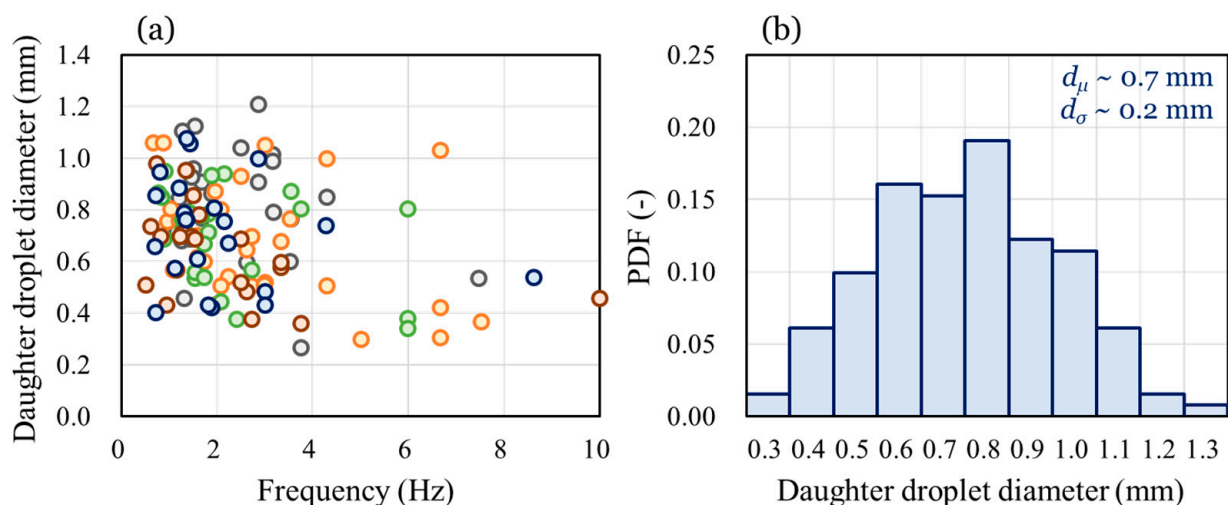


**Figure 6.** Atomization characteristics of the fingering instability. (**a**) Generation frequency of the daughter droplets for five representative fingers during the spreading process; each finger can be distinguished by the plot color. (**b**) PDF histogram for experimental data in (**a**). The number of samples was 131.

## 4. Conclusions

We experimentally investigated the spontaneous spreading and fingering instability of binary droplets on sunflower oil. The droplets released from a 40 wt% IPA solution exhibited spontaneous spreading and fingering instability and underwent a pinch-off process. The spreading behavior of the 40 wt% IPA solution was quantitatively studied. The linear decrease in the brightness of the spreading film could be due to evaporation of the IPA component in the spreading binary liquid film. This evaporation-induced Marangoni force drives the spreading and shrinking processes by temporarily changing the surface tension of the spreading film. We identified the interplay between the spreading diameter

and number of fingers for fingering instability on the spreading front. To elucidate the instability mechanism, the characteristic circumferential and radial lengths of the spreading front are discussed. In the circumferential direction, the capillary length for the IPA solution–sunflower oil interface can reasonably characterized the wavelength between the fingers. In the radial direction, the pinch-off process is described by the classical Plateau–Rayleigh instability of the liquid cylinders. Our experimental results agreed with the theoretical results. The final feature of the fingering instability phenomenon is the pinch-off dynamics. Owing to fingering instability, a myriad of tiny droplets was produced. Most daughter droplets measured less than 1 mm and had frequencies in the range 1–4 Hz. Thus, the generated daughter droplets were distributed across hundreds of micrometers. For the entire spreading film, this spontaneous pinch-off process enables the generation of myriad daughter droplets using a simple sequence.

Although we attempted to characterize the fingering dynamics on the spreading front of the binary droplets on the oil pool as described above, it was difficult to quantify the flow field induced by the Marangoni effect. The flow field in a spreading micrometer-thick film on an oil pool can play an important role in the inception of fingering instability; however, this is beyond the scope of this study. To achieve this, the flow fields within the thin film during the spreading and evaporation of the IPA components must be visualized. This investigation represents a step toward understanding and predicting the fingering instability dynamics of spreading binary droplets on an oil pool to develop a promising atomization technology.

**Author Contributions:** Conceptualization, K.H.; methodology, Y.K.; formal analysis, Y.K. and K.H.; resources, K.H.; writing—original draft preparation, K.H.; writing—review and editing, K.H.; supervision, K.H. All authors have read and agreed to the published version of the manuscript.

**Institutional Review Board Statement:** Not applicable.

**Informed Consent Statement:** Not applicable.

**Data Availability Statement:** The data presented in this study are available upon request from the corresponding author.

**Conflicts of Interest:** The authors declare no conflict of interest.

## References

1.  De Gennes, P.G.; Brochard-Wyart, F.; Quéré, D. *Capillarity and Wetting Phenomena: Drops, Bubbles, Pearls, Waves*; Springer: New York, NY, USA, 2004.
2.  Troian, S.M.; Wu, X.L.; Safran, S.A. Fingering instability in thin wetting films. *Phys. Rev. Lett.* **1989**, *62*, 1496. [CrossRef] [PubMed]
3.  Cazabat, A.M.; Heslot, F.; Troian, S.M.; Carles, P. Fingering instability of thin spreading films driven by temperature gradients. *Nature* **1990**, *346*, 824–826. [CrossRef]
4.  Neitzel, G.P.; Dell'Aversana, P. Noncoalescence and nonwetting behavior of liquids. *Annu. Rev. Fluid. Mech.* **2002**, *34*, 267–289. [CrossRef]
5.  Yarin, A.L. Drop impact dynamics: Splashing, spreading, receding, bouncing. *Annu. Rev. Fluid. Mech.* **2006**, *38*, 159–192. [CrossRef]
6.  Venerus, D.C.; Nieto Simavilla, D. Tears of wine: New insights on an old phenomenon. *Sci. Rep.* **2015**, *5*, 16162. [CrossRef] [PubMed]
7.  Nikolov, A.; Wasan, D.; Lee, J. Tears of wine: The dance of the droplets. *Adv. Colloid Interface Sci.* **2018**, *256*, 94–100. [CrossRef] [PubMed]
8.  Lohse, D.; Zhang, X. Physicochemical hydrodynamics of droplets out of equilibrium. *Nat. Rev. Phys.* **2020**, *2*, 426–443. [CrossRef]
9.  Wang, Z.; Orejon, D.; Takata, Y.; Sefiane, K. Wetting and evaporation of multicomponent droplets. *Phys. Rep.* **2022**, *960*, 1–37. [CrossRef]
10. Cira, N.J.; Benusiglio, A.; Prakash, M. Vapour-mediated sensing and motility in two-component droplets. *Nature* **2015**, *519*, 446–450. [CrossRef]
11. Sanatkaran, N.; Kulichikhin, V.G.; Malkin, A.Y.; Foudazi, R. Spreading of oil-in-water emulsions on water surface. *Langmuir* **2018**, *34*, 10974–10983. [CrossRef]

12. Wodlei, F.; Sebilleau, J.; Magnaudet, J.; Pimienta, V. Marangoni-driven flower-like patterning of an evaporating drop spreading on a liquid substrate. *Nat. Commun.* **2018**, *9*, 820. [CrossRef] [PubMed]

13. Motaghian, M.; Shirsavar, R.; Erfanifam, M.; Sabouhi, M.; Van Der Linden, E.; Stone, H.A.; Bonn, D.; Habibi, M. Rapid spreading of a droplet on a thin soap film. *Langmuir* **2019**, *35*, 14855–14860. [CrossRef] [PubMed]

14. Fanton, X.; Cazabat, A.M. Spreading and instabilities induced by a solutal Marangoni effect. *Langmuir* **1998**, *14*, 2554–2561. [CrossRef]

15. Deodhar, S.; Thampi, S.P.; Basavaraj, M.G. Drops spreading on fluid surfaces: Transition from Laplace to Marangoni regime. *Phys. Rev. Fluids* **2021**, *6*, L112001. [CrossRef]

16. Jia, F.; Wang, T.; Peng, X.; Sun, K. Three stages of Marangoni-driven film spreading for miscible fluids. *Phys. Fluids* **2022**, *34*, 121705. [CrossRef]

17. Motaghian, M.; van der Linden, E.; Habibi, M. Surfactant-surfactant interactions govern unusual Marangoni spreading on a soap film. *Colloids Surf. A Physicochem. Eng. Asp.* **2022**, *653*, 129747. [CrossRef]

18. Baumgartner, D.A.; Shiri, S.; Sinha, S.; Karpitschka, S.; Cira, N.J. Marangoni spreading and contracting three-component droplets on completely wetting surfaces. *Proc. Natl. Acad. Sci. USA* **2022**, *119*, e2120432119. [CrossRef]

19. Liu, D.; Tran, T. Vapor-induced attraction of floating droplets. *J. Phys. Chem. Lett.* **2018**, *9*, 4771–4775. [CrossRef]

20. Mouat, A.P.; Wood, C.E.; Pye, J.E.; Burton, J.C. Tuning contact line dynamics and deposition patterns in volatile liquid mixtures. *Phys. Rev. Lett.* **2020**, *124*, 064502. [CrossRef]

21. Troian, S.M.; Herbolzheimer, E.; Safran, S.A.; Joanny, J.F. Fingering instabilities of driven spreading films. *Europhys. Lett.* **1989**, *10*, 25–30. [CrossRef]

22. Dussaud, A.D.; Troian, S.M. Dynamics of spontaneous spreading with evaporation on a deep fluid layer. *Phys. Fluids* **1998**, *10*, 23–38. [CrossRef]

23. Darhuber, A.A.; Troian, S.M. Marangoni driven structures in thin film flows. *Phys. Fluids* **2003**, *15*, S9. [CrossRef]

24. Dussaud, A.D.; Matar, O.K.; Troian, S.M. Spreading characteristics of an insoluble surfactant film on a thin liquid layer: Comparison between theory and experiment. *J. Fluid Mech.* **2005**, *544*, 23–51. [CrossRef]

25. Keiser, L.; Bense, H.; Colinet, P.; Bico, J.; Reyssat, E. Marangoni bursting: Evaporation-induced emulsification of binary mixtures on a liquid layer. *Phys. Rev. Lett.* **2017**, *118*, 074504. [CrossRef] [PubMed]

26. Kim, H.; Muller, K.; Shardt, O.; Afkhami, S.; Stone, H.A. Solutal Marangoni flows of miscible liquids drive transport without surface contamination. *Nat. Phys.* **2017**, *13*, 1105–1110. [CrossRef]

27. Pinto, R.L.; Le Roux, S.; Cantat, I.; Saint-Jalmes, A. Enhanced interfacial deformation in a Marangoni flow: A measure of the dynamical surface tension. *Phys. Rev. Fluids* **2018**, *3*, 024003. [CrossRef]

28. Kim, S.; Kim, J.; Kim, H.Y. Dewetting of liquid film via vapour-mediated Marangoni effect. *J. Fluid Mech.* **2019**, *872*, 100–114. [CrossRef]

29. Ma, X.; Zhong, M.; He, Y.; Liu, Z.; Li, Z. Fingering instability in Marangoni spreading on a deep layer of polymer solution. *Phys. Fluids* **2020**, *32*, 112112. [CrossRef]

30. Néel, B.; Villermaux, E. The spontaneous puncture of thick liquid films. *J. Fluid Mech.* **2018**, *838*, 192–221. [CrossRef]

31. Aljedaani, A.B.; Wang, C.; Jetly, A.; Thoroddsen, S.T. Experiments on the breakup of drop-impact crowns by Marangoni holes. *J. Fluid Mech.* **2018**, *844*, 162–186. [CrossRef]

32. Villermaux, E. Fragmentation versus cohesion. *J. Fluid Mech.* **2020**, *898*, P1. [CrossRef]

33. Hasegawa, K.; Manzaki, Y. Marangoni fireworks: Atomization dynamics of binary droplets on an oil pool. *Phys. Fluids* **2021**, *33*, 034124. [CrossRef]

34. Zhao, W.; Ma, H.; Ji, W.; Li, W.; Wang, J.; Yuan, Q.; Wang, Y.; Lan, D. Marangoni-driven instability patterns of an N-hexadecane drop triggered by assistant solvent. *Phys. Fluids* **2021**, *33*, 024104. [CrossRef]

35. Matar, O.K.; Troian, S.M. Linear stability analysis of an insoluble surfactant monolayer spreading on a thin liquid film. *Phys. Fluids* **1997**, *9*, 3645–3657. [CrossRef]

36. Schmitt, M.; Stark, H. Marangoni flow at droplet interfaces: Three-dimensional solution and applications. *Phys. Fluids* **2016**, *28*, 012106. [CrossRef]

37. Pototsky, A.; Thiele, U.; Stark, H. Mode instabilities and dynamic patterns in a colony of self-propelled surfactant particles covering a thin liquid layer. *Eur. Phys. J. E* **2016**, *39*, 51. [CrossRef]

38. Sergievskaya, I.; Ermakov, S.; Lazareva, T.; Guo, J. Damping of surface waves due to crude oil/oil emulsion films on water. *Mar. Pollut. Bull.* **2019**, *146*, 206–214. [CrossRef]

39. Ermakov, S.A.; Sergievskaya, I.A.; Gushchin, L.A. Damping of gravity-capillary waves in the presence of oil slicks according to data from laboratory and numerical experiments. *Izv. Atmos. Ocean. Phys.* **2012**, *48*, 565–572. [CrossRef]

40. Rajan, G.K. Dissipation of interfacial Marangoni waves and their resonance with capillary-gravity waves. *Int. J. Eng. Sci.* **2020**, *154*, 103340. [CrossRef]

41. Rajan, G.K. Solutions of a comprehensive dispersion relation for waves at the elastic interface of two viscous fluids. *Eur. J. Mech. B Fluids* **2021**, *89*, 241–258. [CrossRef]

42. Stetten, A.Z.; Moraca, G.; Corcoran, T.E.; Tristram-Nagle, S.; Garoff, S.; Przybycien, T.M.; Tilton, R.D. Enabling Marangoni flow at air-liquid interfaces through deposition of aerosolized lipid dispersions. *J. Colloid Interface Sci.* **2016**, *484*, 270–278. [CrossRef] [PubMed]

43.    Japan Society of Mechanical Engineers (JSME). *JSME Data Book: Thermophysical Properties of Fluids*; JSME: Tokyo, Japan, 1983.
44.    Rosen, M.J. *Surfactants and Interfacial Phenomena*; John Wiley & Sons: Hoboken, NJ, USA, 2004.
45.    Mesyats, G.A.; Zubarev, N.M. The Rayleigh–Plateau instability and jet formation during the extrusion of liquid metal from craters in a vacuum arc cathode spot. *J. Appl. Phys.* **2015**, *117*, 043302. [CrossRef]